

# Localising the Seizure Onset Zone from Single-Pulse Electrical Stimulation Responses with a Transformer

Jamie Norris<sup>1,2</sup>, Aswin Chari<sup>3,4</sup>, Gerald Cooray<sup>5</sup>, Martin Tisdall<sup>3,4</sup>, Karl Friston<sup>1</sup>, Richard Rosch<sup>1,6,7</sup>

<sup>1</sup>Wellcome Centre for Human Neuroimaging, UCL Queen Square Institute of Neurology, London, UK

<sup>2</sup>UCL Institute of Health Informatics, London, UK

<sup>3</sup>Department of Neurosurgery, Great Ormond Street Hospital, London, UK

<sup>4</sup>Developmental Neuroscience, Institute of Child Health, University College London, London, UK

<sup>5</sup>Department of Neurophysiology, Great Ormond Street Hospital, London, UK

<sup>6</sup>Departments of Neurology and Pediatrics, Columbia University, New York, UK

<sup>7</sup>Department of Neurophysiology, King's College Hospital NHS Foundation Trust, London, UK

## Abstract

Epilepsy is one of the most common neurological disorders, and many patients require surgical intervention when medication fails to control seizures. For effective surgical outcomes, precise localisation of the epileptogenic focus – often approximated through the Seizure Onset Zone (SOZ) – is critical yet remains a challenge. Active probing through electrical stimulation is already standard clinical practice for identifying epileptogenic areas. This paper advances the application of deep learning for SOZ localisation using Single Pulse Electrical Stimulation (SPES) responses. We achieve this by introducing Transformer models that incorporate cross-channel attention. We evaluate these models on held-out patient test sets to assess their generalisability to unseen patients and electrode placements.

Our study makes three key contributions: Firstly, we implement an existing deep learning model to compare two SPES analysis paradigms—namely, *divergent* and *convergent*. These paradigms evaluate outward and inward effective connections, respectively. Our findings reveal a notable improvement in moving from a divergent (AUROC: 0.574) to a convergent approach (AUROC: 0.666), marking the first application of the latter in this context. Secondly, we demonstrate the efficacy of the Transformer models in handling heterogeneous electrode placements, increasing the AUROC to 0.730. Lastly, by incorporating inter-trial variability, we further refine the Transformer models, with an AUROC of 0.745, yielding more consistent predictions across patients.

These advancements provide a deeper insight into SOZ localisation and represent a significant step in modelling subject-specific intracranial EEG electrode placements in SPES. Future work will explore integrating these models into clinical decision-making processes to bridge the gap between deep learning research and practical healthcare applications.

**Data and Code Availability** For this study, we utilised an open-source dataset (van Blooij et al., 2023a), which comprises electrocorticography (ECoG) recordings from 74 patients aged between 4 and 51 years undergoing evaluation for epilepsy surgery. We restricted our analyses to the 35 patients for whom each electrode was labelled as within or outside the SOZ. The dataset is available at <https://openneuro.org/datasets/ds004080>. Further details can be found in Section 4.1. Data preprocessing and model training code are available at [https://github.com/norrisjamie23/Localising\\_SOZ\\_from\\_SPES](https://github.com/norrisjamie23/Localising_SOZ_from_SPES).

**Institutional Review Board (IRB)** As the dataset used in this study is open-source, this study does not require IRB approval.

## 1. Introduction

Epileptic seizures originate from diverse brain networks, exhibiting highly individualised, time-varying interictal and ictal patterns that often require uniquely personalised treatments in order to achieve complete seizure control. Around 1 in 100 people will be diagnosed with epilepsy (Vaughan et al., 2018),

and approximately one-third of cases are resistant to medication (Kalilani et al., 2018). Many of these patients are candidates for surgery, which is a safe and effective treatment option to reduce or altogether eliminate seizures (Wiebe et al., 2001). This approach entails identifying and removing focal brain regions implicated in seizure generation, with the seizure onset zone (SOZ) being the primary clinically identifiable proxy for these critical areas. However, identifying the SOZ requires intracranial recordings of spontaneously occurring seizures. Seizures are comparatively rare events and often require extended hospital stays to capture, incurring high costs and stress for patients. Even with the current gold standard evaluation, outcomes remain comparatively poor in cases requiring invasive intracranial evaluation. Moreover, a putative SOZ is not identified at all in approximately 15% of cases, preventing surgical intervention (UK Children’s Epilepsy Surgery Collaboration et al., 2021).

Rather than solely depending on the passive recording of spontaneous seizures, actively probing the epileptic brain’s circuitry is also part of current clinical standard practice. One such method is single-pulse electrical stimulation (SPES), in which an isolated, brief electrical stimulus is applied to individual intracranial electrode contacts (Matsumoto et al., 2017), and evoked distributed responses are measured across the remaining contacts. SPES serves as a proactive tool in the presurgical evaluation of epilepsy, enabling the testing of specific hypotheses about the excitability of targeted regions, with some correlation with their epileptogenicity.

SPES elicits two primary types of responses: early and delayed. Early responses, emerging within 100ms post-stimulation and time-locked to the stimulus, are termed cortico-cortical evoked potentials (CCEPs) (Figure 1D). These CCEPs signify directed or effective connectivity; for instance, if site A is stimulated, a CCEP observed at site B indicates directed neural propagation from A to B. While CCEPs occur in epileptogenic and non-epileptogenic tissue, their characteristics reflect the proximity of the stimulation and recording sites to the SOZ (Hays et al., 2023). However, the common practice of averaging CCEPs across repeated trials (typically 10-50) to enhance the signal-to-noise ratio risks obscuring significant inter-trial variability. This variability could be a crucial indicator of epileptogenicity in specific brain regions (Cornblath et al., 2023).

In contrast, delayed responses, which occur between 100ms and 1s post-stimulation and resemble epileptiform discharges, reflect focal cortical irritability or even epileptogenicity (Figure 1B). These responses have been reported in patients with temporal and frontal lobe epilepsies, and the removal of sites exhibiting these is associated with overall favourable outcomes (Valentín et al., 2005). Unlike the consistent and time-locked nature of CCEPs, delayed responses are neither consistent across trials nor time-locked to the stimulus, meaning they are less apparent when averaging across trials.

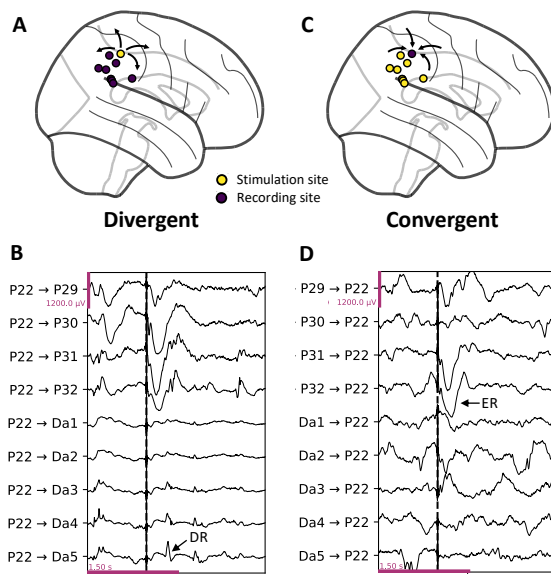


Figure 1: **SPES analysis paradigms.** **A:** Example stimulation and recording sites under a *divergent* paradigm. Example responses are shown in **B**. The same is shown for a *convergent* paradigm in **C** and **D**. A delayed response is shown with an arrow in **B**, and an early response (ER) is shown in **D**. For **B** and **D**,  $A \rightarrow B$  corresponds to the response at electrode B upon stimulation at A.

Recent advances in machine learning, particularly in deep learning, are well-positioned to model complex multidimensional time-series data, such as those generated by SPES. This capability makes deep learning methods particularly promising for integrating multi-channel SPES responses to localise the

SOZ. However, determining the most effective approach to leverage these advanced techniques remains a significant challenge due to particular data features, such as subject-specific electrode placement and variability in the background EEG activity. This leads to several crucial questions for refining and enhancing these methodologies needing to be answered.

In this work, we first address the question of the appropriate analysis paradigm for multi-channel SPES data. An individual node  $S$  can be classified based on its outward connections, i.e., how other sites respond to stimulation at  $S$ . This *divergent* paradigm (Miller et al., 2021) is commonplace and has previously been employed for SOZ localisation (Johnson et al., 2022). Alternatively, individual nodes can be classified based on their inward connections, i.e., how they respond to stimulation at other sites. This *convergent* paradigm is particularly relevant for identifying delayed responses since these are associated with epileptogenic response sites rather than epileptogenic stimulation sites. This approach aligns with findings from Hays et al. (2023), where responses at SOZ sites upon stimulation at non-SOZ sites were more significant than vice-versa, especially at higher currents, suggesting that the *convergent* paradigm could provide a more effective means for SOZ localisation.

A second area of exploration involves integrating information across multiple SPES trials. Classifying individual trials results in numerous predictions for each site. Opting to average across trials addresses this issue. Whilst this averaging process enhances the signal-to-noise ratio, it risks obscuring delayed responses and other important forms of cross-trial variability. Consequently, there is a need for a method that integrates information across trials and effectively factors in this variability.

Lastly, effectively modelling subject-specific and heterogeneous multi-channel data presents a significant challenge. Most machine learning applications to time-series data assume a fixed number of channels with consistent ordering. However, intracranial EEG data varies in channel numbers and placements across patients, impeding model generalisability. Therefore, developing methods that can accommodate the unique and complex nature of subject-specific intracranial EEG datasets is an essential issue that needs to be addressed.

This paper introduces Transformer models with cross-channel attention aimed at enhancing generalisability to unseen patients and managing the com-

plexities of intracranial EEG data. Our study focuses on:

- Adapting an existing deep learning model to compare *divergent* and *convergent* paradigms for SOZ localisation, revealing that switching to a convergent approach improved the AUROC from 0.574 to 0.666.
- Implementing and evaluating Transformer models, outperforming existing methods with an AUROC of 0.730.
- Refining the Transformer models to incorporate inter-trial variability, further increasing the AUROC to 0.745, demonstrating enhanced robustness and precision.

The rest of this paper is organised as follows: We first review related work on SOZ localisation from SPES and Transformers in intracranial EEG. This is followed by our methodology, detailing the various models employed in this study. The experiments section then introduces the dataset and outlines the comparative analysis. This is followed by the results section, which presents our findings. The paper concludes with a discussion of these findings and our concluding remarks.

## 2. Related Work

### 2.1. Localising the SOZ from SPES responses

Malone et al. (2022) evaluated various machine learning algorithms for localising the SOZ from SPES responses, classifying single-channel responses based on whether the recording electrode was in the SOZ. The most effective methods included a 1D convolutional neural network, a gradient-boosted decision tree, and an ensemble approach. In a different study, Yang et al. (2024) focused on computing various CCEP features to classify both stimulated and recording electrodes as SOZ/non-SOZ. These methods, however, consider each channel in isolation, leading to multiple predictions per channel and thereby not integrating the multidimensional data features into the classification. In contrast, Johnson et al. (2022) adopted a multi-channel approach using a divergent paradigm with a ResNet convolutional neural network. This method classifies the stimulated stereo-EEG (SEEG) channel based on responses from other channels. A limitation of this approach is that the network architecture chosen for this analysis requires a consistent

number of channels and associates parameters with specific channel positions. To mitigate this, the authors randomly selected a subset of 40 channels for each pass, sorting these channels based on their proximity to the stimulated electrode. This method’s generalisability was validated using leave-one-out cross-validation. While this approach is suited to extracting temporal features, its effectiveness could benefit from adopting a more sophisticated method to focus on important response channels. Rather than having parameters associated with each of a fixed number of channels, capturing a context-aware representation across all channels may deal better with the heterogeneity of subject-specific seizure networks. Furthermore, this fixed channel count necessitates balancing the model’s prediction accuracy and generalisability.

## 2.2. Transformers for Intracranial EEG

Transformers are a class of deep learning architecture built upon the self-attention mechanism (Vaswani et al., 2017; Bahdanau et al., 2014). Initially proposed in the context of natural language processing (NLP), Transformers have since been applied in a range of domains, including computer vision (Dosovitskiy et al., 2020), reinforcement learning (Chen et al., 2021), and time series (Lim et al., 2021). In NLP, attention mechanisms efficiently encode sequential information across word tokens. This concept is extendable to time series analysis, where attention can instead be applied across temporal sequences. In the context of epilepsy, Transformers have predominantly been applied to electrophysiological data for seizure detection and prediction (Hussein et al., 2022).

Beyond modelling temporal dependencies, Transformers can compute attention between channels, treating each EEG electrode as a token to capture a global context. Encoder-only models, such as BERT (Devlin et al., 2018) and the Vision Transformer (Dosovitskiy et al., 2020), offer flexibility in handling a variable number of tokens due to the utilisation of a class token that represents aggregated information across all tokens. These characteristics may be advantageous in extracting features across channels in intracranial EEG, where the number and placement of electrodes are highly heterogeneous across patients.

An illustrative example is provided by Brant, a foundational model explicitly developed for the analysis of intracranial EEG (Zhang et al., 2024). This model integrates spatial (cross-channel) and tempo-

ral attention mechanisms, enabling it to generalise effectively across various downstream tasks, including neural signal forecasting and seizure detection. However, it remains an open question whether such approaches can accurately model evoked responses, such as those generated by SPES.

## 3. Methods

### 3.1. Notation

To describe each network, we use the following notation. The output for a given stimulation trial is denoted as  $x_d \in \mathbb{R}^{N \times C_{d,i} \times T}$  for the divergent paradigm, and  $x_c \in \mathbb{R}^{N \times C_{c,i} \times T}$  for the convergent paradigm. Here,  $N$  represents the number of trials,  $C_{d,i}$  (or  $C_{c,i}$  for a convergent paradigm) indicates the number of channels for patient  $i$ , and  $T$  is the number of time points. Averaging these responses across trials results in  $\bar{x} \in \mathbb{R}^{C_i \times T}$ , which enhances the signal-to-noise ratio and facilitates a single prediction per electrode. Similarly, the standard deviation across trials is represented as  $S_x \in \mathbb{R}^{C_i \times T}$ , capturing the variability across trials.

### 3.2. Models

We compare the following model architectures:

1. **CNN<sub>divergent</sub>**  
A multi-scale 1D variant (Wang et al., 2018) of a ResNet convolutional neural network (He et al., 2016)<sup>1</sup>.
2. **CNN<sub>convergent</sub>**  
The same architecture as CNN<sub>divergent</sub>, but using a *convergent* paradigm instead of a *divergent* paradigm.
3. **Transformer<sub>base</sub>**  
An encoder-only Transformer (Vaswani et al., 2017) with cross-channel attention. A *convergent* paradigm was used.
4. **Transformer<sub>all</sub>**  
An extension to Transformer<sub>base</sub> with additional input features.

1. <https://github.com/geekfeiw/Multi-Scale-1D-ResNet>

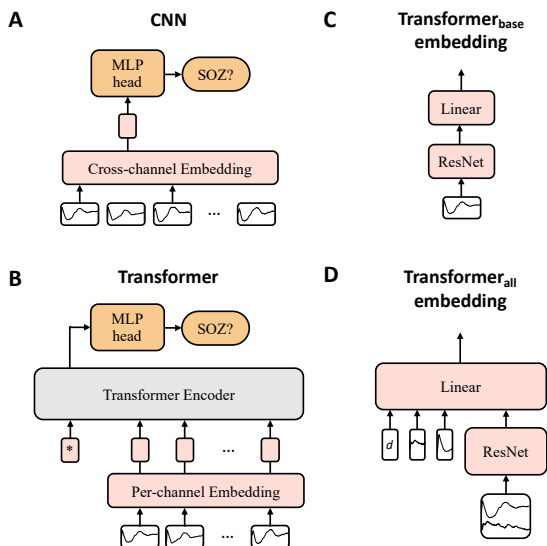


Figure 2: **Network architectures.** **A:** CNN. A ResNet creates a cross-channel embedding, and a multi-layer perceptron (MLP) classifies this as being in or out of the Seizure Onset Zone (SOZ). **B:** Encoder-only Transformer with cross-channel attention. **C:** Embedding for Transformer<sub>base</sub>. **D:** Embedding for Transformer<sub>all</sub>.

### 3.2.1. CNN<sub>DIVERGENT</sub>

To establish a baseline in our study, we first implemented the method previously applied by Johnson et al. (2022) for the same task. Specifically, the authors used a multi-scale 1D ResNet convolutional neural network. ResNets help mitigate overfitting through residual connections, and the multi-scale architecture allows the model to learn features at various temporal scales.

In their study, Johnson et al. (2022) adopted a divergent paradigm, where the objective is to classify a stimulating electrode based on the evoked responses,  $x_d$ , at other electrodes. As described in section 2.1, a random subset of 40 channels were selected during each training and inference pass and arranged in ascending order of distance from the stimulating electrode.

Two modifications were implemented in this approach. Firstly, the number of input channels was treated as a hyperparameter, explicitly optimised for

the current dataset. Secondly, we averaged the responses across trials; that is, we sampled the input from  $\bar{x}_d$ . The channels, randomly selected from  $\bar{x}_d$ , were processed by the network to generate a singular embedding. A multi-layer perceptron subsequently classified this embedding, as depicted in Figure 2A.

### 3.2.2. CNN<sub>CONVERGENT</sub>

To facilitate a comparative analysis of both paradigms, we subsequently trained CNNs using a convergent paradigm. In this approach, we sample the model from  $\bar{x}_c$ , with the number of selected channels again set as a model hyperparameter. As discussed in section 1, this approach is potentially more suited for the task, given that stimulation from non-SOZ to SOZ sites results in larger responses than vice versa and that delayed responses occur at epileptogenic response sites. However, it was unclear if delayed responses would be detected, given that averaging across trials attenuates their prominence. Apart from these differences, the model architecture remained consistent with CNN<sub>divergent</sub>, as detailed in Figure 2A.

### 3.2.3. TRANSFORMER<sub>BASE</sub>

We next implemented encoder-only Transformer models with cross-channel attention, as introduced in Section 2.2. We opt for a convergent paradigm, enabling a direct comparison with CNN<sub>convergent</sub>. Unlike the CNN models, the Transformer model does not require a fixed number of channels, thus allowing it to process responses from all channels. The network is depicted in Figure (Figure 2B). For embeddings, a multi-scale 1D ResNet – as with CNN<sub>convergent</sub> – was employed; however, this process was conducted independently for each channel, leading to a distinct embedding per channel (Figure 2C).

These embeddings are then subjected to spatial attention, facilitating integration across channels. This process learns a representation across all channels, drawing on the context provided by their interactions. This strategy overcomes the limitations of fixed channel inputs and enables the model to weigh channels based on their features without making assumptions based on the channel order.

### 3.2.4. TRANSFORMER<sub>ALL</sub>

To overcome certain limitations of Transformer<sub>base</sub>, we developed an extended version, Transformer<sub>all</sub>

(Figure 2D). We made several modifications to enhance SOZ localisation capabilities:

Firstly, given the potential relationship between inter-trial variability and epileptogenicity (Cornblath et al., 2023) and that delayed responses are inconsistent across trials, we hypothesised that averaging across trials might obscure crucial data. To address this, we incorporated standard deviation across trials ( $S_{x_c}$ ) alongside the mean ( $\bar{x}_c$ ) as part of the model’s input. Each channel was represented as a 2D input to the CNN, combining both time series.

Secondly, since CNNs have some degree of shift-invariance, time-locked responses like CCEPs might not be optimally captured. To mitigate this, we introduced an additional branch in our per-channel embedding. Specifically, the first 300ms of both  $\bar{x}_c$  and  $S_{x_c}$  – corresponding to the CCEP component – were directly concatenated to the CNN output (Figure 2D). By skipping the CNN, the linear layer directly embeds the CCEP, which has no shift-invariance.

Lastly, the physical distance between stimulating and response sites was identified as a potentially informative feature for SOZ localisation. For instance, large CCEP amplitudes observed over varying distances, not just between nearby channels, could indicate epileptogenicity. Therefore, we included the distance between recording and response sites as an additional feature in the model.

## 4. Experiments

### 4.1. Dataset

Details of the dataset are included in the Data and Code Availability section. The ECoG data were recorded at a sampling rate of 2048 Hz, and these patients exhibited a wide range of seizure onset locations, spanning various regions across the brain. Stimulation was performed at 0.2 Hz with a current intensity of 4mA or 8mA. For additional information on the dataset, including the number and distribution of electrode locations, see Appendix A.

### 4.2. Dataset split

We employed repeated k-fold cross-validation with  $k = 5$  and 5 repeats. To assess model generalisability to new patients and ECoG electrode locations, each patient was present in one fold, ensuring no patient data overlap between the training and testing sets. Further details are provided in Appendix B.

### 4.3. Preprocessing

Data were first bandpass filtered to 1-150 Hz in line with previous work in the same task (Johnson et al., 2022). Further preprocessing was applied in line with previous work using the same dataset (van Blooij et al., 2023b), as outlined in Appendix C.

### 4.4. Evaluation criteria

To assess model performance across repeated k-fold cross-validation, we employed both threshold-independent and threshold-dependent metrics, each computed per patient and then averaged across patients, folds, and repeats. We used the Area Under the Receiver Operating Characteristic (AUROC) and the Area Under the Precision-Recall Curve (AUPRC) for threshold-independent metrics. We report the specificity, sensitivity, and Youden’s index (Youden, 1950) for threshold-dependent metrics, which consider binary rather than continuous predictions. We also report the p-value testing for an increase in model performance from  $\text{CNN}_{\text{convergent}}$  to  $\text{Transformer}_{\text{base}}$ . Further details are included in Appendix D.

### 4.5. Hyperparameter tuning

We undertook a hyperparameter search for each model using Optuna (Akiba et al., 2019) to ensure that observed differences in model performance were not due to inadequate hyperparameter configurations. This process led to the selection of 49 channels for  $\text{CNN}_{\text{divergent}}$  and 37 channels for  $\text{CNN}_{\text{convergent}}$ . Further details of the hyperparameter search spaces and the chosen hyperparameters for each model are in Appendix E.

### 4.6. Channel sensitivity analysis

Although the rationale for adopting a Transformer over a CNN is its potential to extract features from relevant channels more effectively, it is worth considering the extent to which the performance of  $\text{Transformer}_{\text{base}}$  could be attributed to the availability of more channels during inference. If this were the case, it would indicate that cross-channel attention is not the cause of these improvements. To investigate this aspect, we undertook a sensitivity analysis with  $\text{Transformer}_{\text{base}}$ , focusing on how its performance depends on the number of channels available during inference.

Table 1: **Model Performance Metrics.** Mean and standard deviation of the AUROC, AUPRC, specificity, sensitivity, and Youden’s index for each model across all test folds and runs. The baseline AUPRC, based on the prevalence of the positive class, is 0.136.

Model	AUROC	AUPRC	Specificity	Sensitivity	Youden
CNN <sub>divergent</sub>	$0.574 \pm 0.065$	$0.204 \pm 0.056$	$0.598 \pm 0.205$	$0.500 \pm 0.199$	$0.098 \pm 0.105$
CNN <sub>convergent</sub>	$0.666 \pm 0.067$	$0.305 \pm 0.074$	$0.671 \pm 0.147$	$0.532 \pm 0.214$	$0.202 \pm 0.121$
Transformer <sub>base</sub>	$0.730 \pm 0.082$	$0.377 \pm 0.119$	$0.636 \pm 0.185$	$0.597 \pm 0.267$	$0.233 \pm 0.147$
Transformer <sub>all</sub>	$0.745 \pm 0.098$	$0.378 \pm 0.121$	$0.642 \pm 0.181$	$0.663 \pm 0.212$	$0.305 \pm 0.143$

#### 4.7. Transformer performance in Frontal/Temporal SOZs

One of the motivations for including the standard deviation across trials in Transformer<sub>all</sub> was the potential to better identify delayed responses, which the averaging process could obscure. Since these are observed in the frontal and temporal lobes (Valentín et al., 2005), the patient cohort was divided into two groups for this analysis: those primarily with frontal or temporal lobe SOZs and those without. We computed the AUROC scores for both groups for Transformer<sub>base</sub> and Transformer<sub>all</sub>. The underlying hypothesis was that if the observed improvement in model performance were primarily due to enhanced detection of delayed responses, the improvement would be particularly pronounced in the sub-cohort of patients with a higher incidence of frontal and temporal lobe SOZs.

## 5. Results

### 5.1. Performance metrics

Table 1 presents the performance metrics for each model. CNN<sub>divergent</sub>, previously shown to attain a Youden’s index of 0.527 (Johnson et al., 2022), underperformed in this task, registering a Youden’s index of only 0.098 and an AUROC marginally above chance at 0.574. In comparison, CNN<sub>convergent</sub> had an increased AUROC of 0.666, yet it still faced challenges in generalisation.

We observed improved model performance in Transformer<sub>base</sub>, which attained an AUROC of 0.730. This improvement over CNN<sub>convergent</sub> was statistically significant ( $p = 0.036$ ). Incorporating additional features in Transformer<sub>all</sub> yielded a minor increase in the AUROC to 0.745, though the AUPRC remained almost constant (0.377 to 0.378). While

this suggests only a marginal improvement at the individual patient level – if any – a notable increase in the Youden index from 0.233 to 0.305 was observed, mainly due to a large increase in sensitivity (0.597 to 0.663). This improvement, achieved using a threshold determined from the validation set, points to an enhanced ability of the model to generalise across different patients.

ROC curves for each model are shown in Appendix F.

### 5.2. Channel sensitivity analysis

The channel sensitivity analysis assessed the relationship between Transformer<sub>base</sub> performance and the number of channels used during inference. A crucial finding was the model’s robust performance across varying channel counts, including a monotonic increase in performance with an increasing number of channels, as illustrated in Figure 3.

When the channel count was set to 37, in line with CNN<sub>convergent</sub>, our model achieved an AUROC of 0.724. This performance notably surpassed that of the CNN model, which had an AUROC of 0.666 with the same number of channels. Furthermore, the resilience of Transformer<sub>base</sub> was underscored when the channel count was reduced to just 4, yielding an AUROC of 0.667, equalling that of CNN<sub>convergent</sub>.

### 5.3. Transformer performance in Frontal/Temporal SOZs

This analysis focused on assessing whether the improved performance of Transformer<sub>base</sub> was more pronounced in the cohort with predominantly frontal/temporal lobe SOZs, which could suggest the identification of delayed responses. However, the data did not support an improvement in AUROC scores within this cohort (0.741 to 0.743). Instead, we ob-

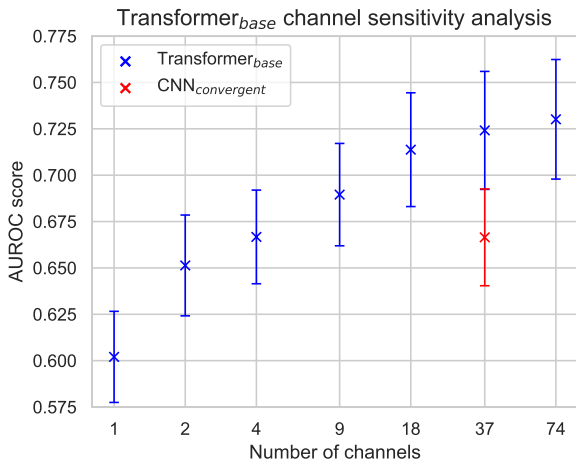


Figure 3: **Channel sensitivity analysis for Transformer<sub>base</sub>.** In this analysis, a random subset of  $n$  channels served as input for each prediction, testing different values of  $n$ . This analysis used the previously trained Transformer<sub>base</sub> models. AUROC scores for CNN<sub>convergent</sub>, which used 37 channels, are presented for comparison. Bootstrapping was used to calculate 95% confidence intervals.

served an overall increase in the mean AUROC in the cohort with a minority of frontal/temporal lobe SOZs (0.702 to 0.750), albeit with overlapping confidence intervals. Figure 4 illustrates these findings.

#### 5.4. Predictions visualised

Example predictions for a single patient are visualised in Figure 5. CNN<sub>convergent</sub> significantly overlaps with the clinician labelled SOZ, albeit with several false positives. Transformer<sub>base</sub> exhibits a similar overlap but with fewer false positives. Notably, Transformer<sub>all</sub> demonstrates the most effective performance, with substantial alignment with the clinician labels, reflecting the superior capabilities of this model.

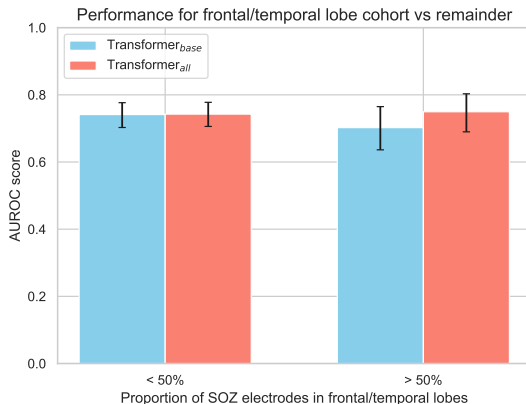


Figure 4: **Frontal/temporal lobe SOZ analysis.** The trained Transformer models were evaluated on two subcohorts: those with a majority of frontal/temporal lobe SOZs and those with a minority. For each of Transformer<sub>base</sub> and Transformer<sub>all</sub>, AUROC scores were calculated across these subcohorts, with 95% confidence intervals calculated using bootstrapping.

## 6. Discussion

### 6.1. Baseline performance

The change in dataset may have led to the suboptimal performance of CNN<sub>divergent</sub>. For instance, the stimulation parameters differed between the two datasets. Johnson et al. (2022) employed a stimulation frequency of 1 Hz, whereas van Blooij et al. (2023a) – whose dataset we use – applied a stimulation frequency of 0.2 Hz. It is plausible that the impaired performance can be attributed to the differences in responses elicited by stimulation at epileptogenic sites between these two frequencies.

The heterogeneity of seizure onsets in this dataset (see Appendix A) compared with the previous focus on temporal lobe epilepsies may have been a contributing factor. Given the limited sample size, this may have led to underfitting. Another possible explanation is that our approach averaged responses across trials, attenuating delayed responses. However, Johnson et al. (2022) reported only a slight decrease in performance when limiting the post-stimulation window to 0-175ms – i.e., removing most delayed responses,



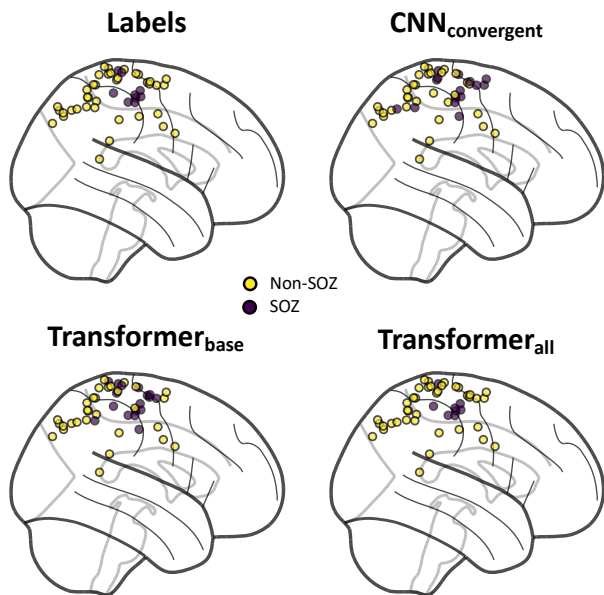


Figure 5: **Model outputs for a single patient.** Electrodes are classified as SOZ or non-SOZ. Nodes represent electrodes; colours denote clinician-determined ground truth (top left) or the prediction for a given model. This patient was absent from the training set, demonstrating model generalisability to unseen patients and electrodes.

suggesting any performance reduction attributable to averaging across trials was likely negligible.

Finally, the dataset’s composition, encompassing patients irrespective of treatment outcome, poses a significant challenge. Similar studies typically concentrate on patients with predominantly positive outcomes. Including patients who experienced unsuccessful treatment outcomes – where the labelled SOZ may not accurately represent true epileptogenicity – could systematically diminish the model’s performance in attempting to infer actual epileptogenic regions.

Given the reduced performance of  $\text{CNN}_{\text{divergent}}$  on the dataset employed in this study, it is desirable to compare our methods on the same dataset used by Johnson et al. (2022). This approach would further validate the generalisability of our findings.

## 6.2. Divergent vs Convergent paradigms

In the introduction, we hypothesised that a *convergent* paradigm might be more conducive to effective SOZ localisation. This hypothesis was premised on the literature suggesting that response sites are more indicative of epileptogenicity than stimulation sites. Our empirical investigation, comparing  $\text{CNN}_{\text{divergent}}$  with  $\text{CNN}_{\text{convergent}}$ , lends credence to this hypothesis. The AUROC increased notably from 0.574 to 0.666, marking a substantial improvement, although this remains low for a task of critical importance.

## 6.3. CNN vs Transformer comparison

In our comparative study of  $\text{CNN}_{\text{convergent}}$  and  $\text{Transformer}_{\text{base}}$ , the latter demonstrated statistically significant superiority. An important question was whether this advantage was solely due to its ability to process all channels during inference rather than just a subset. Section 5.2 shows evidence to the contrary, where  $\text{Transformer}_{\text{base}}$  outperformed  $\text{CNN}_{\text{convergent}}$  even when restricted to the same number of inference channels.

The Transformer’s cross-channel attention mechanism enables improved feature extraction compared to  $\text{CNN}_{\text{convergent}}$ , which applies a ResNet to compute a single set of features across channels. The superiority of the Transformer lies in its ability to extract channel-wise features and then apply cross-channel attention, explaining the performance disparity between the two models. Recent evidence has demonstrated the efficacy of cross-channel attention in intracranial EEG analysis (Zhang et al., 2024). Our findings further extend its applicability, demonstrating its ability to model evoked responses effectively. Given the heterogeneity in subject-specific electrode configurations and its high spatial resolution, intracranial EEG is particularly well-suited to benefit from this mechanism.

## 6.4. Additional Transformer features

The lack of improvement in the frontal/temporal lobe SOZ cohort for  $\text{Transformer}_{\text{all}}$  suggests a lack of improvement in detecting delayed responses. Had this been the case, we would expect an increase in performance in this cohort, given that delayed responses are seen in these regions (Valentín et al., 2005). Unless  $\text{Transformer}_{\text{base}}$  is already adept at detecting delayed responses, this indicates the potential need for a more sophisticated approach to detect such responses. For

instance, a method that explicitly considers all trials might be required instead of relying on summary statistics across trials.

It is worth considering why AUROC scores for the remainder of the cohort may have improved. Firstly, the standard deviation may reflect other forms of inter-trial variability, which Cornblath et al. (2023) suggests could possess predictive power in identifying epileptogenic tissue. Secondly, as discussed in Section 3.2.4, the addition of an extra branch in the per-channel embedding might have enhanced the discrimination between epileptogenic and non-epileptogenic CCEPs. Finally, incorporating the distance between stimulating and recording electrodes as a feature may have contributed to this increased generalisability.

### 6.5. Limitations and future work

A fundamental limitation of our models is that even the best-performing method, `Transformerconvergent`, only has a Youden score of 0.305. Without considering patient outcomes, it is difficult to know the true capability of these methods, as patients with poor outcomes would likely have a significant impact on model performance. Future work should aim to train models on patients with favourable outcomes and compare the performance between unseen patients with bad and good outcomes. Improved performance on patients with favourable outcomes would indicate that these models are more indicative of epileptogenic regions than SOZ labels alone.

Another challenge is the limited scope of our models’ validation, which is confined to patients from the same dataset. Whilst we evaluated generalisability to unseen patients and electrode placements, our evaluation did not test for generalisability to other centres, a fundamental limitation given the variability in stimulation protocols and electrode modality (ECoG or SEEG). To validate their generalisability convincingly, testing on an external dataset is paramount. Ideally, such testing should be preceded by training models on a dataset derived from a multi-centre cohort, thus ensuring model robustness across clinical environments.

Aligning our strategy with clinical practice is another area for development. Clinical practice incorporates diverse data, including seizure activity, interictal recordings, magnetic resonance and PET imaging, and other clinical information. This integration takes place during multidisciplinary team meetings through discussions and visual comparisons. A multi-

modal machine learning approach, utilising extensive, high-quality data, could significantly improve model performance, assuming complexity and scalability issues are overcome (Kline et al., 2022).

Explainability is paramount in healthcare applications, where comprehending models’ decision-making processes is critical. The reliance on complex ‘black box’ models accentuates the necessity for explainable methodologies. Integrated gradients (Sundararajan et al., 2017) represent one such approach. This method can verify that data artefacts do not improperly influence decisions by highlighting salient SPES responses. Such transparency is crucial for affirming model reliability and clinical applicability.

Finally, as discussed in section 6.4, our approach of using summary statistics across trials is likely sub-optimal. While this method captures some inter-trial variability whilst increasing the signal-to-noise ratio of CCEPs, it may only partially capture trial-by-trial variability, obscuring trends over time. Learning directly across trials could provide a more nuanced understanding of these responses.

## 7. Conclusion

This paper presents several contributions for modelling intracranial EEG data using deep learning, particularly in localising the SOZ from SPES data. Our research first compares *divergent* and *convergent* paradigms in classifying multi-channel SPES responses. This comparison revealed a substantial improvement in moving from the conventional divergent approach (AUROC: 0.574) to a convergent one (AUROC: 0.666).

Moreover, we have pioneered the use of Transformer models in analysing SPES responses. Our approach of applying a Transformer with cross-channel attention to invasive EEG data has shown promising results, elevating the AUROC to 0.730. Further refinement of this model by incorporating features such as inter-trial variability led to an increased AUROC of 0.745, demonstrating more consistent predictions across patients.

We aim to extend our work in several directions. One key area is investigating whether our approach can predict epileptogenicity more accurately than traditional SOZ localisation by considering patient outcomes. Another avenue is to explore the potential of the Transformer model to process SPES responses across trials rather than using summary statistics. Additionally, evaluating our model on an external

dataset will be crucial, given the heterogeneity in SPES protocols.

Our research marks a notable advancement in modelling subject-specific, heterogeneous intracranial EEG placements in SPES. Through the application of deep learning methodologies, we strive to make a meaningful contribution towards enhancing surgical outcomes for individuals with drug-resistant epilepsy.

## References

- Takuya Akiba, Shotaro Sano, Toshihiko Yanase, Takeru Ohta, and Masanori Koyama. Optuna: A next-generation hyperparameter optimization framework. In *Proceedings of the 25th ACM SIGKDD international conference on knowledge discovery & data mining*, pages 2623–2631, 2019.
- Dzmitry Bahdanau, Kyunghyun Cho, and Yoshua Bengio. Neural machine translation by jointly learning to align and translate. *arXiv preprint arXiv:1409.0473*, 2014.
- Lili Chen, Kevin Lu, Aravind Rajeswaran, Kimin Lee, Aditya Grover, Misha Laskin, Pieter Abbeel, Aravind Srinivas, and Igor Mordatch. Decision transformer: Reinforcement learning via sequence modeling. *Advances in neural information processing systems*, 34:15084–15097, 2021.
- Eli J Cornblath, Alfredo Lucas, Caren Armstrong, Adam S Greenblatt, Joel M Stein, Peter N Hadar, Ramya Raghupathi, Eric Marsh, Brian Litt, Kathryn A Davis, et al. Quantifying trial-by-trial variability during cortico-cortical evoked potential mapping of epileptogenic tissue. *Epilepsia*, 2023.
- Jacob Devlin, Ming-Wei Chang, Kenton Lee, and Kristina Toutanova. Bert: Pre-training of deep bidirectional transformers for language understanding. *arXiv preprint arXiv:1810.04805*, 2018.
- Alexey Dosovitskiy, Lucas Beyer, Alexander Kolesnikov, Dirk Weissenborn, Xiaohua Zhai, Thomas Unterthiner, Mostafa Dehghani, Matthias Minderer, Georg Heigold, Sylvain Gelly, et al. An image is worth 16x16 words: Transformers for image recognition at scale. *arXiv preprint arXiv:2010.11929*, 2020.
- Mark A Hays, Rachel J Smith, Yujing Wang, Christopher Coogan, Sridevi V Sarma, Nathan E Crone, and Joon Y Kang. Cortico-cortical evoked potentials in response to varying stimulation intensity improves seizure localization. *Clinical Neurophysiology*, 145:119–128, 2023.
- Kaiming He, Xiangyu Zhang, Shaoqing Ren, and Jian Sun. Deep residual learning for image recognition. In *Proceedings of the IEEE conference on computer vision and pattern recognition*, pages 770–778, 2016.
- Ramy Hussein, Soojin Lee, and Rabab Ward. Multi-channel vision transformer for epileptic seizure prediction. *Biomedicines*, 10(7):1551, 2022.
- Graham W Johnson, Leon Y Cai, Derek J Doss, Jasmine W Jiang, Aarushi S Negi, Saramati Narasimhan, Danika L Paulo, Hernán FJ González, Shawniqua Williams Roberson, Sarah K Bick, et al. Localizing seizure onset zones in surgical epilepsy with neurostimulation deep learning. *Journal of Neurosurgery*, 138(4):1002–1007, 2022.
- Linda Kalilani, Xuezheng Sun, Barbara Pelgrims, Matthias Noack-Rink, and Vicente Villanueva. The epidemiology of drug-resistant epilepsy: a systematic review and meta-analysis. *Epilepsia*, 59(12):2179–2193, 2018.
- Adrienne Kline, Hanyin Wang, Yikuan Li, Saya Dennis, Meghan Hutch, Zhenxing Xu, Fei Wang, Feixiong Cheng, and Yuan Luo. Multimodal machine learning in precision health. *arXiv preprint arXiv:2204.04777*, 2022.
- Bryan Lim, Sercan Ö Arık, Nicolas Loeff, and Tomas Pfister. Temporal fusion transformers for interpretable multi-horizon time series forecasting. *International Journal of Forecasting*, 37(4):1748–1764, 2021.
- Ilya Loshchilov and Frank Hutter. Decoupled weight decay regularization. *arXiv preprint arXiv:1711.05101*, 2017.
- Ian G Malone, Kaleb E Smith, Morgan E Urdaneta, Tyler S Davis, Daria Nesterovich Anderson, Brian J Phillip, John D Rolston, and Christopher R Butson. Machine learning methods applied to cortico-cortical evoked potentials aid in localizing seizure onset zones. *arXiv preprint arXiv:2211.07867*, 2022.

- Riki Matsumoto, Takeharu Kunieda, and Dileep Nair. Single pulse electrical stimulation to probe functional and pathological connectivity in epilepsy. *Seizure*, 44:27–36, 2017.
- Kai J Miller, Klaus-Robert Müller, and Dora Hermes. Basis profile curve identification to understand electrical stimulation effects in human brain networks. *PLoS computational biology*, 17(9):e1008710, 2021.
- Claude Nadeau and Yoshua Bengio. Inference for the generalization error. *Advances in neural information processing systems*, 12, 1999.
- Adam Paszke, Sam Gross, Francisco Massa, Adam Lerer, James Bradbury, Gregory Chanan, Trevor Killeen, Zeming Lin, Natalia Gimelshein, Luca Antiga, et al. Pytorch: An imperative style, high-performance deep learning library. *Advances in neural information processing systems*, 32, 2019.
- Mukund Sundararajan, Ankur Taly, and Qiqi Yan. Axiomatic attribution for deep networks. In *International conference on machine learning*, pages 3319–3328. PMLR, 2017.
- UK Children’s Epilepsy Surgery Collaboration, Aswin Chari, Friederike Moeller, Stewart Boyd, M Zubair Tahir, J Helen Cross, Christin Eltze, Krishna Das, Thijs van Dalen, Rod C Scott, et al. The uk experience of stereoelectroencephalography in children: An analysis of factors predicting the identification of a seizure-onset zone and subsequent seizure freedom. *Epilepsia*, 62(8):1883–1896, 2021.
- Antonio Valentín, Gonzalo Alarcón, Mrinalini Honavar, Jorge J García Seoane, Richard P Selway, Charles E Polkey, and Colin D Binnie. Single pulse electrical stimulation for identification of structural abnormalities and prediction of seizure outcome after epilepsy surgery: a prospective study. *The Lancet Neurology*, 4(11):718–726, 2005.
- D. van Blooijis, M.A. van den Boom, J.F. van der Aar, G.J.M. Huiskamp, G. Castegnaro, M. Demuru, W.J.E.M. Zweiphenning, P. van Eijnsden, K. J. Miller, F.S.S. Leijten, and D. Hermes. ”ccep ecog dataset across age 4-51”, 2023a.
- Dorien van Blooijis, Max A van den Boom, Jaap F van der Aar, Geertjan M Huiskamp, Giulio Castegnaro, Matteo Demuru, Willemiek JEM Zweiphenning, Pieter van Eijnsden, Kai J Miller, Frans SS Leijten, et al. Developmental trajectory of transmission speed in the human brain. *Nature Neuroscience*, 26(4):537–541, 2023b.
- Ashish Vaswani, Noam Shazeer, Niki Parmar, Jakob Uszkoreit, Llion Jones, Aidan N Gomez, Lukasz Kaiser, and Illia Polosukhin. Attention is all you need. *Advances in neural information processing systems*, 30, 2017.
- Kerry A Vaughan, Christian Lopez Ramos, Vivek P Buch, Rania A Mekary, Julia R Amundson, Meghal Shah, Abbas Rattani, Michael C Dewan, and Kee B Park. An estimation of global volume of surgically treatable epilepsy based on a systematic review and meta-analysis of epilepsy. *Journal of neurosurgery*, 130(4):1127–1141, 2018.
- Fei Wang, Jinsong Han, Shiyuan Zhang, Xu He, and Dong Huang. Csi-net: Unified body characterization and action recognition. *arXiv preprint arXiv:1810.03064*, 2018.
- Samuel Wiebe, Warren T Blume, John P Girvin, and Michael Eliasziw. A randomized, controlled trial of surgery for temporal-lobe epilepsy. *New England Journal of Medicine*, 345(5):311–318, 2001.
- Bowen Yang, Baotian Zhao, Chao Li, Jiajie Mo, Zhihao Guo, Zilin Li, Yuan Yao, Xiuliang Fan, Du Cai, Lin Sang, et al. Localizing seizure onset zone by a cortico-cortical evoked potentials-based machine learning approach in focal epilepsy. *Clinical Neurophysiology*, 2024.
- William J Youden. Index for rating diagnostic tests. *Cancer*, 3(1):32–35, 1950.
- Daoze Zhang, Zhizhang Yuan, Yang Yang, Junru Chen, Jingjing Wang, and Yafeng Li. Brant: Foundation model for intracranial neural signal. *Advances in Neural Information Processing Systems*, 36, 2024.

## Appendix A. Dataset

The processed dataset comprises 2066 electrodes, averaging 59 per patient. These were restricted to stimulated electrodes to facilitate a fair comparison between both paradigms. Among these electrodes, 298 (14.4%) were identified as within the SOZ. The electrode location distribution, including those within the

SOZ, was consistent across lobes (Figure 6), indicating that brain regions are unlikely to significantly confound the results.

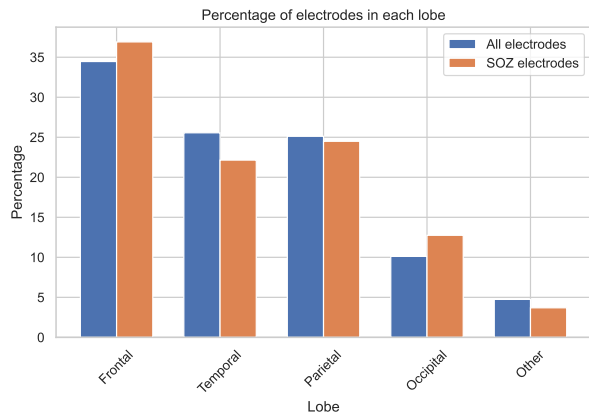


Figure 6: **Electrode distribution across lobes.** This figure presents the percentage of all electrodes in each lobe versus those within the SOZ. It shows that the SOZ electrodes follow a similar distribution to all electrodes.

## Appendix B. Dataset split

We repeated the following five times, each with a different random seed. We divided the dataset at the patient level into  $k = 5$  folds, such that all data for a given patient was in one fold only. In every run, we used three of these folds for training, one for validation, and one for testing. This approach was chosen to balance computational resource demands and the need for reliable model evaluation.

## Appendix C. Preprocessing

Firstly, we corrected each stimulation epoch for baseline by removing the mean from a preceding 900ms window (-1s to -0.1s). As stimulation artefact can spread through volume conductance effects, we removed the first 9ms post-stimulation and any electrodes within 13mm of the stimulated electrode. As known responses to SPES mainly occur within 1s, this window was maintained such that each epoch was (9ms, 1s) post-stimulation.

After dividing the dataset into training, validation, and test sets for each run, we carried out standardisation to ensure zero mean and unit standard deviation. This process involved computing the mean and standard deviation across the training set. We used these calculated parameters from the training set to independently standardise the training, validation, and test sets to prevent data leakage.

During training, we added noise with zero mean and a standard deviation of 0.1 for data augmentation. We removed a subset of channels during each training pass for the Transformer models, with a proportion uniformly distributed from  $[0, 0.5]$ .

## Appendix D. Metrics

The AUROC and AUPRC scores consider class imbalance, with AUPRC being particularly effective in imbalanced dataset scenarios. These metrics indicate, at the patient level, whether SOZ electrodes are generally scored higher than non-SOZ electrodes.

A threshold was required to compute the specificity, sensitivity, and Youden’s index. For each model, the optimal threshold was determined on the validation set to maximise Youden’s index and then applied to the corresponding test set. This approach assesses the practicality of using a consistent, patient-independent threshold and evaluates if the model’s ability to distinguish between SOZ and non-SOZ channels holds across different patients.

The statistical test between  $\text{CNN}_{\text{convergent}}$  and  $\text{Transformer}_{\text{base}}$  was a one-sided t-test using [Nadeau and Bengio \(1999\)](#)’s corrected method for repeated k-fold cross-validation. We calculated the p-value based on the mean AUROC scores from each fold and run, with a significance threshold set at 0.05.

## Appendix E. Model training procedures

Models were trained in PyTorch ([Paszke et al., 2019](#)). An AdamW optimiser was used for training ([Loshchilov and Hutter, 2017](#)) with a binary cross-entropy loss function. The *pos\_weight* argument was used to account for class imbalance. The default parameters were used, except for the learning rate, which was determined through the hyperparameter search. For the CNN models, the search space was as follows: (1) learning rate within  $[1 \times 10^{-4}, 1 \times 10^{-2}]$ , (2) dropout rate at the fully connected layer within  $[0,$

0.5], (3) number of input trials, an integer from [20, 80]. For the Transformer models, this search space was: (1) learning rate within  $[1 \times 10^{-4}, 1 \times 10^{-2}]$ , (2) dropout rate after the embedding layer, in the Transformer layers, and at the fully connected layer within  $[0, 0.5]$ , (3) embedding dimension from  $\{16, 32, 64\}$ , (4) Transformer layers from  $\{1, 2\}$ . The number of Transformer heads was set to  $1/8$  of the embedding dimension. These search spaces were determined based on initial experiments on the validation sets.

Ten trials were conducted for each model, a decision aimed at balancing model performance against the constraints of computational resources. Training was halted after ten epochs, and the set of hyperparameters that maximised the validation AUROC were selected. This process was only done once, with a separate random seed to the 5 runs, as this process took several times longer than the final model training. The best hyperparameters for the CNN and Transformer models are shown in Tables 2 and 3, respectively.

## Appendix F. ROC curves

Each model’s Receiver Operating Characteristic (ROC) curves are shown in Figure 7, summarising the trade-off between sensitivity and specificity across various threshold settings. Consistent with the AUROC scores, the convergent paradigm outperformed the divergent paradigm across thresholds, and the Transformer models demonstrated superior performance compared to the CNN models. However, the ROC curves for the Transformer models displayed a notable similarity. In summary, these curves illustrate the superior discrimination ability of the Transformer models.

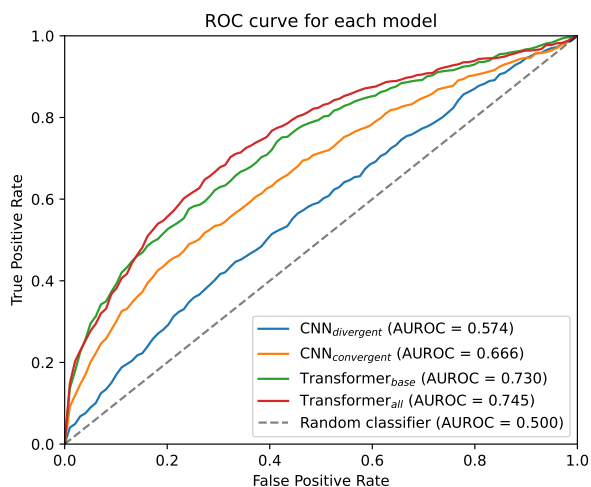


Figure 7: **ROC Curves for each model.** Receiver Operating Characteristic (ROC) curves are shown for each model alongside a baseline random classifier. The AUROC scores are indicated for each model.

Table 2: **Hyperparameters for CNN Models.** The table displays the optimal dropout rate and input channels for both CNN models as determined by the hyperparameter search.

Model	Dropout Rate	Input Channels	Learning rate
CNN <sub>divergent</sub>	0.22	49	$4.0 \times 10^{-3}$
CNN <sub>convergent</sub>	0.44	37	$1.3 \times 10^{-3}$

Table 3: **Hyperparameters for Transformer Models.** The table presents the optimal dropout rate, embedding dimension, and number of layers for both Transformer models as determined by the hyperparameter search.

Model	Dropout Rate	Embedding Dim	Num Layers	Learning rate
Transformer <sub>base</sub>	0.46	16	2	$1.5 \times 10^{-4}$
Transformer <sub>all</sub>	0.44	16	2	$3.4 \times 10^{-3}$